

Confronting $h \rightarrow Z\gamma$ Excess with the Two Higgs Doublet Model

Feng-Zhi Chen, Qiaoyi Wen, and Fanrong Xu*

*Department of Physics, College of Physics & Optoelectronic Engineering,
Jinan University, Guangzhou 510632, P.R. China*

Abstract

The approximately 2σ deviation from the Standard Model (SM) prediction in the Higgs decay channel $h \rightarrow Z\gamma$ suggests a potential avenue for new physics. In contrast, the precisely measured value of $h \rightarrow \gamma\gamma$, which is consistent with the SM prediction, places stringent constraints on new physics parameters, especially considering the correlation between these two decay modes. In this study, we propose a new mechanism and provide a complete analytical calculation in the context of the flavor-gauged two Higgs doublet model (FG2HDM), where a novel type of coupling between the charged Higgs and vector bosons can selectively affect the $h \rightarrow Z\gamma$ decay without altering $h \rightarrow \gamma\gamma$. However, due to the smallness of the constrained model parameters, additional modifications are required: to adjust the involved Z boson-fermion vertices, extra fermions such as technifermions must be introduced into the model. We show that the FG2HDM, along with the inclusion of new fermions, can simultaneously accommodate the 1σ measured intervals for both $\mu_{Z\gamma}$ and $\mu_{\gamma\gamma}$, offering a consistent explanation for both decay modes.

* fanrongxu@jnu.edu.cn

I. INTRODUCTION

The discovery of the Higgs boson at the Large Hadron Collider (LHC) by the ATLAS and CMS collaborations in 2012 marked a significant triumph for the SM [1–3]. Since then, the quest for new physics (NP) beyond the SM (BSM) has been one of the central endeavors in elementary particle physics. A primary approach involves measuring the Higgs decays, as any significant deviation of observations from SM predictions can serve as a clear indication of NP.

Recently, the ATLAS and CMS collaborations announced the initial evidence for $h \rightarrow Z\gamma$ decay, with the signal strength observed at the 68% confidence level (CL) being $\mu_{Z\gamma}^{\text{ATLAS}} = 2.0_{-0.9}^{+1.0}$ for the ATLAS analysis [4] and $\mu_{Z\gamma}^{\text{CMS}} = 2.4 \pm 0.9$ for the CMS analysis [5], and $\mu_{Z\gamma}^{\text{Exp}} = 2.2 \pm 0.7$ for their combination [6].¹ Interestingly, the combined signal strength slightly deviates from its SM prediction $\mu_{Z\gamma}^{\text{SM}} = 1$ at the level of 1.9σ , which, if confirmed, would be a clear signal of NP beyond the SM. Explanations for this discrepancy are primarily sought in two main areas. On the one hand, given that the $h \rightarrow Z\gamma$ decay is loop-induced, it is essential to account for higher-order corrections to the leading-order (LO) contributions from one-loop amplitudes. Two categories of corrections have been calculated: the two-loop QCD corrections [7–10], which contribute approximately a 0.3% increase, and the two-loop electroweak corrections [11, 12], resulting in a 7% enhancement. Clearly, these next-to-leading-order (NLO) corrections alone are inadequate to explain the 1.9σ deviation. On the other hand, the excess may be attributed to additional contributions from the BSM physics, which have been extensively explored in numerous studies, see, e.g., Refs. [13–29].

When analyzing the $h \rightarrow Z\gamma$ decay in a specific BSM model, it is also common to consider the $h \rightarrow \gamma\gamma$ decay, since any charged particles that contribute at the loop level to the former can also influence the latter [30, 31]. Interestingly, unlike the case for $\mu_{Z\gamma}$, the experimental value for the $h \rightarrow \gamma\gamma$ decay, $\mu_{\gamma\gamma}^{\text{Exp}} = 1.10 \pm 0.06$ [32], is in good concordance with the SM prediction $\mu_{\gamma\gamma}^{\text{SM}} = 1$. This suggests that, for a given model, the parameters accounting for the excess of the $h \rightarrow Z\gamma$ must also adhere to the stringent constraint imposed by the $h \rightarrow \gamma\gamma$ decay, i.e., they should exclusively contribute to $\mu_{Z\gamma}$ without altering $\mu_{\gamma\gamma}$. Note that the flavor is always conserved in the QED, which, however, may be violated

¹ In Refs. [4–6] the signal strength μ_X (X is any Higgs decay product) is defined as the product of the cross section and the branch fraction ($\sigma(pp \rightarrow h)\mathcal{B}(h \rightarrow X)$) relative to the SM prediction. The cross section aligns well with the SM prediction, so we assumed that the NP merely affect the branching fractions.

during the scalar and weak interactions. Thus, a plausible hypothesis is to construct a BSM model featuring off-diagonal couplings between the Higgs and Z boson with the intermediate particles. This approach has been explored, e.g., in Refs. [16, 19]. In this study, we propose a novel mechanism to achieve the same goal by introducing a new neutral gauge boson Z' , which mixes with the Z boson but not with the photon, producing new corrections to the couplings of the Z boson and fermions that exclusively affect $\mu_{Z\gamma}$ without modifying $\mu_{\gamma\gamma}$. By adjusting the magnitude of these corrections, it is possible to reconcile the $\mu_{Z\gamma}$ excess.

Note that the decays $h \rightarrow Z\gamma$ (as well as $h \rightarrow \gamma\gamma$) have already been examined within a specific two Higgs doublet model (2HDM) (see Ref. [33] for a comprehensive review on the general 2HDM), namely the complex 2HDM (C2HDM) [34], with parameters constrained based on earlier measurements reported by the ATLAS [35] and CMS [36]. With the new results from Refs. [4–6], however, both model construction and numerical analysis require further refinement. Intriguingly, both the off-diagonal couplings of the Higgs and Z boson and corrections to the Z boson-fermion couplings can be implemented in the so-called FG2HDM, which is constructed based on the Branco-Grimus-Lavoura (BGL) type 2HDM [37] (see also the subsequent developments in Refs. [38–41]) and has been utilized to address the B anomalies in our previous work [42]. In the FG2HDM, the original 2HDM is extended by an additional scalar singlet and endowed with a gauged $U(1)$ flavor symmetry (which we dub as $U(1)'$ hereafter) to suppress the occurrence of undesired tree-level flavor-changing neutral currents (FCNCs). Compared to the SM particle spectrum, the FG2HDM features five additional physical scalars and one additional neutral gauge boson Z' . In this work, we calculate the one-loop amplitudes for the decays $h \rightarrow Z\gamma$ and $h \rightarrow \gamma\gamma$ and explore how these two signal strengths can be simultaneously reconciled within the framework of the FG2HDM.

The rest of the paper is organized as follows. In Sec. II, we provide a brief overview of the key features of the FG2HDM. In Sec. III, we calculate the one-loop amplitudes for $h \rightarrow Z\gamma$ and $h \rightarrow \gamma\gamma$ decays in the unitary gauge. The numerical analysis and subsequent discussions are detailed in Sec. IV. Our conclusion is presented in Sec. V. For convenience, the relevant Lagrangian and the corresponding Feynman rules are prepared in Appendix A. Additionally, the explicit expressions for the scalar functions obtained from one-loop calculations are listed in Appendix B, along with the kinematics for Higgs decays in Appendix C.

II. THE MODEL

The FG2HDM is a specific 2HDM comprising two $SU(2)_L$ scalar doublets, extended by an additional scalar singlet S , and endowed with a $U(1)'$ gauge symmetry. The scalar potential is given by [42]

$$\begin{aligned}
V(\Phi_1, \Phi_2, S) = & m_{11}^2 \Phi_1^\dagger \Phi_1 + m_{22}^2 \Phi_2^\dagger \Phi_2 + \frac{\lambda_1}{2} (\Phi_1^\dagger \Phi_1)^2 + \frac{\lambda_2}{2} (\Phi_2^\dagger \Phi_2)^2 \\
& + \lambda_3 (\Phi_1^\dagger \Phi_1) (\Phi_2^\dagger \Phi_2) + \lambda_4 (\Phi_1^\dagger \Phi_2) (\Phi_2^\dagger \Phi_1) \\
& + m_S^2 |S|^2 + \lambda_S |S|^4 + \kappa_1 |\Phi_1|^2 |S|^2 + \kappa_2 |\Phi_2|^2 |S|^2 \\
& + \kappa_3 \left(\Phi_1^\dagger \Phi_2 S^2 + \Phi_2^\dagger \Phi_1 (S^*)^2 \right), \tag{1}
\end{aligned}$$

where $m_{11,22,S}$ represent the quadratic parameters, and $\lambda_{1,2,3,4,S}$ along with $\kappa_{1,2,3}$ denote the quartic couplings. The two doublets and the singlet in the flavor basis are parametrized as:

$$\Phi_1 = \begin{pmatrix} \phi_1^+ \\ \frac{1}{\sqrt{2}}(\rho_1 + i\eta_1 + v_1) \end{pmatrix}, \quad \Phi_2 = \begin{pmatrix} \phi_2^+ \\ \frac{1}{\sqrt{2}}(\rho_2 + i\eta_2 + v_2) \end{pmatrix}, \quad S = \frac{1}{\sqrt{2}}(s_0 + i\chi_0 + v_S), \tag{2}$$

where the vacuum expectation values (VEVs) v_1 and v_2 combine to form the SM Higgs VEV $v = 1/(\sqrt{2}G_F)^{1/2} = \sqrt{v_1^2 + v_2^2} \simeq 246$ GeV, with G_F being the Fermion constant. The singlet VEV v_S is introduced to spontaneously break the $U(1)'$ symmetry. Rotating to the mass basis yields:

$$\begin{pmatrix} G^\pm \\ H^\pm \end{pmatrix} = U_1 \begin{pmatrix} \phi_1^\pm \\ \phi_2^\pm \end{pmatrix}, \quad \begin{pmatrix} G^0 \\ G'^0 \\ H_A \end{pmatrix} = U_2 \begin{pmatrix} \eta_1 \\ \eta_2 \\ \chi_0 \end{pmatrix}, \quad \begin{pmatrix} H \\ h \\ H_S \end{pmatrix} = U_3 \begin{pmatrix} \rho_1 \\ \rho_2 \\ s_0 \end{pmatrix}, \tag{3}$$

where U_1 , U_2 , and U_3 are the rotation matrices defined as:

$$U_1 \equiv \begin{pmatrix} \cos \beta & \sin \beta \\ -\sin \beta & \cos \beta \end{pmatrix}, \quad U_2 \equiv \begin{pmatrix} 1 & 0 \\ 0 & U_\gamma \end{pmatrix} \begin{pmatrix} U_1 & 0 \\ 0 & 1 \end{pmatrix}, \quad U_3 \equiv \begin{pmatrix} -\cos \alpha & -\sin \alpha & 0 \\ \sin \alpha & -\cos \alpha & 0 \\ 0 & 0 & 1 \end{pmatrix}. \tag{4}$$

Here, α and β are the rotation angles, and the 2×2 matrix U_γ and $\tan 2\alpha$ are given by:

$$U_\gamma = \begin{pmatrix} \frac{2v_1 v_2}{\sqrt{4v_1^2 v_2^2 + v^2 v_S^2}} & \frac{-v v_S}{\sqrt{4v_1^2 v_2^2 + v^2 v_S^2}} \\ \frac{v v_S}{\sqrt{4v_1^2 v_2^2 + v^2 v_S^2}} & \frac{2v_1 v_2}{\sqrt{4v_1^2 v_2^2 + v^2 v_S^2}} \end{pmatrix}, \quad \tan 2\alpha = \frac{2l}{m - n}, \tag{5}$$

where

$$m = \lambda_1 v_1^2 - \frac{1}{2} \kappa_3 \frac{v_2}{v_1} v_S^2, \quad n = \lambda_2 v_2^2 - \frac{1}{2} \kappa_3 \frac{v_1}{v_2} v_S^2, \quad l = \lambda_{34} v_1 v_2 + \frac{1}{2} \kappa_3 v_S^2. \quad (6)$$

After spontaneous symmetries breaking, the four undesired Goldstone bosons G^\pm , G^0 and G'^0 in Eq. (3) would get ‘eaten’ to give masses to the W^\pm , Z , and Z' gauge bosons, respectively. This leaves us with six physical scalars: two charged Higgs H^\pm , three neutral scalars H , h , and H_S , and one neutral pseudoscalar H_A . Their masses are separately given by

$$\begin{aligned} m_{h,H}^2 &= \frac{1}{2} \left[(m+n) \mp \sqrt{(m-n)^2 + 4l^2} \right], & m_{H_S}^2 &= 2\lambda_S v_S^2, \\ m_{H_A}^2 &= -\frac{1}{2} \kappa_3 \left(4v_1 v_2 + \frac{v^2 v_S^2}{v_1 v_2} \right), & m_{H^\pm}^2 &= -\frac{1}{2} \left(\lambda_4 v^2 + \frac{\kappa_3 v^2 v_S^2}{v_1 v_2} \right). \end{aligned} \quad (7)$$

Among the three neutral particles, h and H are CP-even, while H_A is CP-odd. Specially, the scalar h is identified as the Higgs boson discovered at the LHC in 2012 [1–3].

Regarding the neutral gauge bosons, the covariant derivatives for the $SU(2)_L$ doublet and singlet fields are defined as follows:

$$D_\mu = \partial_\mu - ig_1 Y_i B_\mu - ig' X_i \hat{Z}'_\mu - ig_2 \frac{\vec{\tau}}{2} \cdot \vec{W}_\mu, \quad (8)$$

$$D_\mu = \partial_\mu - ig_1 Y_i B_\mu - ig' X_i \hat{Z}'_\mu, \quad (9)$$

where $\vec{\tau}$ are the Pauli matrices, and B_μ , \hat{Z}'_μ , and \vec{W}_μ are the $U(1)_Y$, $U(1)'$ and $SU(2)_L$ gauge bosons in the flavor basis, respectively. Here, g_1 , g' , g_2 are the corresponding coupling constants, while Y_i and X_i denote separately the hypercharge and $U(1)'$ charge of the fields. After spontaneous symmetry breaking, the gauge bosons acquire their masses. The transformation from the flavor basis to the mass basis is achieved through the mixing matrix:

$$\begin{pmatrix} A \\ Z \\ Z' \end{pmatrix} = U \begin{pmatrix} B \\ W^3 \\ \hat{Z}' \end{pmatrix}, \quad U = \begin{pmatrix} \cos \theta_W & \sin \theta_W & 0 \\ -\sin \theta_W \cos \theta'_2 & \cos \theta_W \cos \theta'_2 & \sin \theta'_2 \\ \sin \theta_W \sin \theta'_2 & -\cos \theta_W \sin \theta'_2 & \cos \theta'_2 \end{pmatrix}, \quad (10)$$

where θ_W is the Weinberg angle, and θ'_2 the mixing angle between Z and Z' . In the limit where θ'_2 approaches zero, the mixing restores to the case in the SM. This arrangement introduces the tree-level FCNCs in the down-type quark sector, which can account for the anomalies observed in B physics [42]. Additionally, it generates off-diagonal interactions,

with Higgs and Z boson couple to charged Higgs and W boson, and new corrections to the Z boson-fermion couplings, which are essential for addressing the $\mu_{Z\gamma}$ discrepancy in this work.

In Table I, we have collected the quantum numbers for the various fields within the FG2HDM framework under the $SU(3)_C \times SU(2)_L \times U(1)_Y \times U(1)'$ symmetries. The $U(1)'$ charges, denoted as X_i ($i = L_L, \dots, S$), are assigned to ensure the cancellation of $U(1)'$ gauge anomalies. The specific relationships among the $U(1)'$ charges for different fields are elaborated in Appendix A of Ref. [42]. It is noteworthy that the anomaly-free condition can be achieved through various Yukawa texture assignments for quarks and leptons, as further discussed in Refs. [39–41].

Fields	L_L	e_R	Q_L	u_R	d_R	Φ_1	Φ_2	S
$SU(3)_C$	1	1	3	3	3	1	1	1
$SU(2)_L$	2	1	2	1	1	2	2	1
$U(1)_Y$	$-\frac{1}{2}$	-1	$\frac{1}{6}$	$\frac{2}{3}$	$-\frac{1}{3}$	$\frac{1}{2}$	$\frac{1}{2}$	0
$U(1)'$	X_{L_L}	X_{e_R}	X_{Q_L}	X_{u_R}	X_{d_R}	X_{Φ_1}	X_{Φ_2}	X_S

TABLE I. The quantum numbers of different fields under the $SU(3)_C \times SU(2)_L \times U(1)_Y \times U(1)'$ symmetries. Here, $L_L = (\nu_L, e_L)^T$ and $Q_L = (u_L, d_L)^T$ represent separately the left-handed lepton and quark $SU(2)_L$ doublets, while e_R , u_R , and d_R denote the right-handed lepton, up-type quark, and down-type quark $SU(2)_L$ singlets, respectively.

Armed with the quantum charge assignments for various fields, the FG2HDM Lagrangian can be systematically derived. As detailed in Sec. II of Ref. [42], we opt for brevity in this work and refrain from presenting the full Lagrangian. Instead, we focus on the key terms essential for calculating the one-loop amplitudes of the $h \rightarrow Z\gamma$ and $h \rightarrow \gamma\gamma$ decays. These terms, along with their corresponding Feynman rules, are compiled in Appendix A.

III. ONE-LOOP AMPLITUDES

Following a general Lorentz decomposition while enforcing photon gauge invariance, as detailed in Ref. [9], we can express the amplitudes for the processes $h(p) \rightarrow Z(p_1)\gamma(p_2)$ and

$h(p) \rightarrow \gamma(p_1)\gamma(p_2)$ in the following form:

$$\mathcal{M}_X = (p_2^\mu p_1^\nu - p_1 \cdot p_2 g^{\mu\nu}) T_X \epsilon_\mu^*(p_1) \epsilon_\nu^*(p_2), \quad X = Z\gamma, \gamma\gamma, \quad (11)$$

where $\epsilon_{\mu(\nu)}$ represents the polarization vector of the Z boson or photon, and T_X denotes the one-loop functions to be determined. In the presence of NP, the function T_X can be written as $T_X = T_X^{\text{SM}} + T_X^{\text{NP}}$, and the signal strength μ_X is defined as

$$\mu_X = \left| 1 + \frac{T_X^{\text{NP}}}{T_X^{\text{SM}}} \right|^2. \quad (12)$$

Utilizing the Feynman rules for vertices and propagators outlined in Figure 7 of Appendix A, we can determine the one-loop Feynman diagrams for the decays $h \rightarrow Z\gamma$ and $h \rightarrow \gamma\gamma$, as depicted in Figures 1 and 2. We have omitted the diagrams containing off-diagonal fermions in the loops, given the strong suppression of the FCNCs. Upon examining the Feynman diagrams for $h \rightarrow Z\gamma$ and $h \rightarrow \gamma\gamma$, an additional class of diagrams with off-diagonal couplings to the Higgs and Z boson is observed for $h \rightarrow Z\gamma$ (i.e., the last row of Figure 1),² which suggests a greater contribution of the FG2HDM to $h \rightarrow Z\gamma$ relative to $h \rightarrow \gamma\gamma$. Furthermore, the novel corrections to the Z boson-fermion couplings offer an alternative pathway to enhance the contribution to $h \rightarrow Z\gamma$, as previously discussed in Sec. I. The one-loop functions T_X can then be extracted by matching onto the calculations of the one-loop Feynman diagrams. In this work, we will calculate these diagrams with the help of the Mathematica package, *Package-X* [44], details are as follows.

A. $h \rightarrow Z\gamma$

The one-loop Feynman diagrams that contribute to the $h \rightarrow Z\gamma$ process are depicted in Figure 1. We have intentionally omitted the self-energy diagrams for this decay mode because they lack the Lorentz structure specified in Eq. (11), and the divergences present in the calculations of the Feynman diagrams in each row of Figure 1 are found to cancel each other out (a pattern that also applies to $h \rightarrow \gamma\gamma$). These diagrams are categorized into four distinct classes (one row, one class), each corresponding to a type of particle involved in the internal lines. Consequently, the total one-loop function $T_{Z\gamma}$ is decomposed of the following

² Note that such diagrams have ever appeared in other Higgs models, see, e.g., Refs. [30, 43].

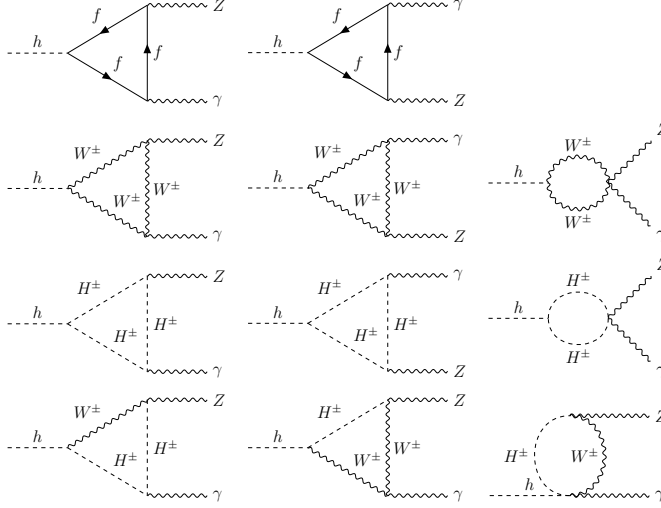


FIG. 1. One-loop Feynman diagrams for $h \rightarrow Z\gamma$.

four distinct components:

$$T_{Z\gamma} = T_{Z\gamma}^f + T_{Z\gamma}^W + T_{Z\gamma}^H + T_{Z\gamma}^{WH}, \quad (13)$$

corresponding to contributions from fermionic, W boson, charged Higgs, and mixed W boson and charged Higgs loops, respectively. Specially,

$$T_{Z\gamma}^f = \sum_f \frac{eg_2 Q_f N_C m_f}{16\pi^2 m_W (m_h^2 - m_Z^2)^2} \left[\frac{g_2}{c_W} (I_f^3 - 2Q_f s_W^2) \cos \theta'_2 + g' (\mathcal{Q}_{fL} + \mathcal{Q}_{fR}) \sin \theta'_2 \right] \\ \times [\sin(\alpha - \beta) M_f - \cos(\alpha - \beta) N_f] \left\{ 4m_Z^2 [\Lambda(m_h^2; m_f, m_f) - \Lambda(m_Z^2; m_f, m_f)] \right. \\ \left. + 2(m_h^2 - m_Z^2) \left[2 + (4m_f^2 - m_h^2 + m_Z^2) C_0(m_Z^2, 0, m_h^2, m_f^2, m_f^2, m_f^2) \right] \right\}, \quad (14)$$

$$T_{Z\gamma}^W = -\frac{eg_2^2 c_W \sin(\alpha - \beta) \cos \theta'_2}{16\pi^2 m_W^3 (m_h^2 - m_Z^2)^2} \left\{ [12m_W^4 - 2m_W^2 m_Z^2 + m_h^2 (2m_W^2 - m_Z^2)] \right. \\ \times \left[(m_h^2 - m_Z^2) + m_Z^2 (\Lambda(m_h^2; m_W, m_W) - \Lambda(m_Z^2; m_W, m_W)) \right] + 2m_W^2 (m_h^2 - m_Z^2) \\ \left. \times (12m_W^4 + 6m_W^2 m_Z^2 - 2m_Z^4 - 6m_h^2 m_W^2 + m_h^2 m_Z^2) C_0(m_Z^2, 0, m_h^2, m_W^2, m_W^2, m_W^2) \right\}, \quad (15)$$

$$T_{Z\gamma}^H = -\frac{4ev\lambda_{hH^+H^-}}{16\pi^2 (m_h^2 - m_Z^2)^2} \left[\left(\frac{g_2}{2} c_W - \frac{g_1}{2} s_W \right) \cos \theta'_2 + (\sin^2 \beta \mathcal{Q}_1 + \cos^2 \beta \mathcal{Q}_2) g' \sin \theta'_2 \right] \\ \times \left\{ m_Z^2 [\Lambda(m_h^2; m_{H^\pm}, m_{H^\pm}) - \Lambda(m_Z^2; m_{H^\pm}, m_{H^\pm})] \right\}$$

$$+(m_h^2 - m_Z^2) \left[1 + 2m_{H^\pm}^2 C_0(m_Z^2, 0, m_h^2, m_{H^\pm}^2, m_{H^\pm}^2, m_{H^\pm}^2) \right] \Big\}, \quad (16)$$

$$\begin{aligned} T_{Z\gamma}^{WH} &= \frac{eg_2g'(\mathcal{Q}_2 - \mathcal{Q}_1) \cos(\alpha - \beta) \sin \beta \cos \beta \sin \theta'_2}{16\pi^2 m_W (m_h^2 - m_Z^2)} \\ &\times \left\{ 2(m_h^2 - m_{H^\pm}^2 + m_W^2) \left[\frac{m_Z^2}{m_h^2 - m_Z^2} (\Lambda(m_h^2; m_{H^\pm}, m_W) - \Lambda(m_Z^2; m_{H^\pm}, m_W)) \right. \right. \\ &+ \left. \frac{m_{H^\pm}^2 - m_W^2}{2m_h^2} \log \left(\frac{m_{H^\pm}^2}{m_W^2} \right) + m_{H^\pm}^2 C_0(0, m_h^2, m_Z^2, m_{H^\pm}^2, m_{H^\pm}^2, m_W^2) + 1 \right] \\ &\left. - 2m_W^2 (m_h^2 + m_{H^\pm}^2 - m_W^2 - 2m_Z^2) C_0(0, m_h^2, m_Z^2, m_W^2, m_W^2, m_{H^\pm}^2) \right\}. \quad (17) \end{aligned}$$

In Eq. (14), we have summed over the contributions from all of the fermions, and the color factor $N_C = 3(1)$ for quarks (leptons). The symbols \mathcal{Q}_{Lf} , \mathcal{Q}_{fR} , \mathcal{Q}_1 , \mathcal{Q}_2 denote the $U(1)'$ charge of left-handed fermion, right-handed fermion, Φ_1 , and Φ_2 , respectively. The analytical expressions for the scalar functions $\Lambda(m_a^2; m_b, m_c)$, $C_0(m_Z^2, 0, m_h^2, m_i^2, m_i^2, m_i^2)$, and $C_0(0, m_h^2, m_Z^2, m_i^2, m_i^2, m_j^2)$ in Eqs. (14)-(17) are listed in Appendix B. Note that similar expressions for T_X can also be found in Ref. [34]. It is worth emphasizing the novel contribution $T_{Z\gamma}^{WH}$, which arises from the $W^\pm H^\mp Z$ coupling and is uniquely present in the FG2HDM, distinguishing it from other conventional 2HDMs.

B. $h \rightarrow \gamma\gamma$

The one-loop Feynman diagrams responsible for the $h \rightarrow \gamma\gamma$ process are illustrated in Figure 2. In the depiction of the first and second diagrams in each row, distinct momenta

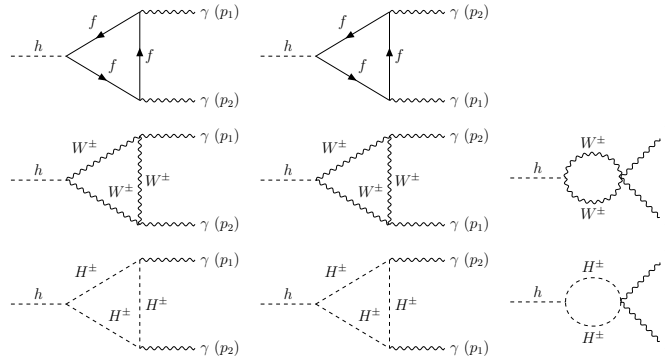


FIG. 2. One-loop Feynman diagrams for $h \rightarrow \gamma\gamma$.

p_1 and p_2 are assigned to differentiate the two photons in the final state. Paralleling the

approach for $h \rightarrow Z\gamma$, the total one-loop function $T_{\gamma\gamma}$ is decomposed into three distinct parts:

$$T_{\gamma\gamma} = T_{\gamma\gamma}^f + T_{\gamma\gamma}^W + T_{\gamma\gamma}^H, \quad (18)$$

with each term explicitly given by:

$$T_{\gamma\gamma}^f = \sum_f \frac{4e^2 g_2 N_C Q_f^2 m_f (\sin(\alpha - \beta) M_f - \cos(\alpha - \beta) N_f)}{16\pi^2 m_h^2 m_W} \times [2 + (4m_f^2 - m_h^2) C_0(0, 0, m_h^2, m_f^2, m_f^2, m_f^2)], \quad (19)$$

$$T_{\gamma\gamma}^W = \frac{-2e^2 g_2 \sin(\alpha - \beta)}{16\pi^2 m_h^2 m_W} [(m_h^2 + 6m_W^2 + (12m_W^4 - 6m_h^2 m_W^2) C_0(0, 0, m_h^2, m_W^2, m_W^2, m_W^2))], \quad (20)$$

$$T_{\gamma\gamma}^H = -\frac{4e^2 v \lambda_{hH^+H^-}}{16\pi^2 m_h^2} [1 + 2m_{H^\pm}^2 C_0(0, 0, m_h^2, m_{H^\pm}^2, m_{H^\pm}^2, m_{H^\pm}^2)]. \quad (21)$$

The analytical expressions for the scalar function $C_0(0, 0, m_h^2, m_i^2, m_i^2, m_i^2)$ in Eqs. (19)-(21) can also be found in Appendix B. Unlike in the $h \rightarrow Z\gamma$ process, there is no $T_{Z\gamma}^{WH}$ contribution because the $W^\pm H^\mp \gamma$ interaction is forbidden in FG2HDM, as it is in other 2HDMs and the SM.

IV. NUMERICAL ANALYSIS

In this section, we perform a numerical analysis to determine whether the FG2HDM can accommodate the measured $\mu_{Z\gamma}$ excess while evading constraints from $\mu_{\gamma\gamma}$. For ease of reference, the input parameters used in the numerical analysis throughout this work are summarized in Table II. It should be noted that the fine structure constant, $\alpha \equiv e^2/4\pi$, is scale dependent and is related to the electroweak gauge coupling g_2 via the relation $e = g_2 \sin \theta_W$. Additionally, we do not adopt the experimental value for Γ_h from the particle data group (PDG), which has a relatively large uncertainty ($\Gamma_h^{\text{PDG}} = 3.7_{-1.4}^{+1.9}$ MeV) [32], but rather, we cite the value with smaller uncertainty from Ref. [45]. Our strategy in this section initially involves calculating the SM LO contributions for the decays $h \rightarrow Z\gamma$ and $h \rightarrow \gamma\gamma$, the numerical values of which provide valuable insights for building NP models. We then incorporate the corrections from the FG2HDM in detail.

$\sin^2 \theta_W = 0.23129(4)$	[32]	$m_W = 80.3692(133)$ GeV	[32]
$\alpha(0) = 1/137.036$	[32]	$m_Z = 91.1880(20)$ GeV	[32]
$\alpha(m_Z) = 1/127.944(14)$	[32]	$m_h = 125.20(11)$ GeV	[32]
$\Gamma_h = 4.07^{+4.0\%}_{-3.9\%}$ MeV	[45]	$m_t = 172.57(29)$ GeV	[32]
$G_F = 1.1663788 \times 10^{-5}$ GeV ⁻²	[32]	$m_\tau = 1.77693(9)$ GeV	[32]
$m_b = 4.183(7)$ GeV	[32]	$m_c = 1.2730(46)$ GeV	[32]
$m_s = 93.5(8)$ MeV	[32]	$m_\mu = 105.658$ MeV	[32]
$m_d = 4.70(7)$ MeV	[32]	$m_e = 0.511$ MeV	[32]
$m_u = 2.16(7)$ MeV	[32]		

TABLE II. Relevant input parameters used in our numerical analysis.

A. SM prediction

The expressions in Eqs. (14)-(17) and (19)-(21) revert to the SM formulas upon setting $\theta'_2 \rightarrow 0$ and $\sin(\alpha - \beta) \rightarrow 1$. The numerical results for $T_{Z\gamma}$ in the SM are then given by:

$$\begin{aligned}
T_{Z\gamma}^{W,\text{SM}} &= -5.866 \times 10^{-5}, & T_{Z\gamma}^{t,\text{SM}} &= 3.115 \times 10^{-6}, \\
T_{Z\gamma}^{b,\text{SM}} &= -6.685 \times 10^{-8} + 3.762 \times 10^{-8}i, & T_{Z\gamma}^{c,\text{SM}} &= -9.797 \times 10^{-9} + 3.864 \times 10^{-9}i, \\
T_{Z\gamma}^{\tau,\text{SM}} &= -1.731 \times 10^{-9} + 7.452 \times 10^{-10}i. & &
\end{aligned} \tag{22}$$

Eq. (22) (and also Eq. (23)) clearly indicates that the dominant contributions arise from the W loops, and the secondary contributions come from the top quark loops. Contributions from the s , d , u , μ , and e loops are not presented here, as they are several orders of magnitude smaller than those we display and can be neglected safely. Likewise, the SM contributions to $T_{\gamma\gamma}$ are

$$\begin{aligned}
T_{\gamma\gamma}^{W,\text{SM}} &= -3.912 \times 10^{-5}, & T_{\gamma\gamma}^{t,\text{SM}} &= 8.619 \times 10^{-6}, \\
T_{\gamma\gamma}^{b,\text{SM}} &= -1.123 \times 10^{-7} + 1.485 \times 10^{-7}i, & T_{\gamma\gamma}^{c,\text{SM}} &= -9.103 \times 10^{-8} + 7.462 \times 10^{-8}i, \\
T_{\gamma\gamma}^{\tau,\text{SM}} &= -1.107 \times 10^{-7} + 1.011 \times 10^{-7}i. & &
\end{aligned} \tag{23}$$

With the kinematics formula derived in Appendix C, the SM predictions for $h \rightarrow Z\gamma$ and $h \rightarrow \gamma\gamma$ are given separately by

$$\mathcal{B}(h \rightarrow Z\gamma)_{\text{SM}} = (1.536 \pm 0.018) \times 10^{-3}, \tag{24}$$

$$\mathcal{B}(h \rightarrow \gamma\gamma)_{\text{SM}} = (2.278 \pm 0.023) \times 10^{-3}, \quad (25)$$

which are respectively in good agreement with those given in Ref. [45]: $\mathcal{B}(h \rightarrow Z\gamma) = (1.5 \pm 0.1) \times 10^{-3}$, and $\mathcal{B}(h \rightarrow \gamma\gamma) = (2.27 \pm 0.07) \times 10^{-3}$. Besides, $\mathcal{B}(h \rightarrow \gamma\gamma)_{\text{SM}}$ (and thus $\mu_{\gamma\gamma}^{\text{SM}}$) also agrees well with the experimental value, $\mathcal{B}(h \rightarrow \gamma\gamma)_{\text{Exp}} = (2.50 \pm 0.20) \times 10^{-3}$ ($\mu_{\gamma\gamma}^{\text{Exp}}$) [32]. However, the SM prediction for $\mathcal{B}(h \rightarrow Z\gamma)_{\text{SM}}$ (and thus $\mu_{Z\gamma}^{\text{SM}}$) deviates from the experimental result $(3.4 \pm 1.1) \times 10^{-3}$ ($\mu_{Z\gamma}^{\text{Exp}} = 2.2 \pm 0.7$) by 1.9σ [6]. As discussed in Sec. I, it is still impossible to account for such a discrepancy even taking into account the NLO contributions, thus, some NP contribution is strongly called for.

B. FG2HDM contributions

The $h \rightarrow \gamma\gamma$ decay imposes stringent constraints on the FG2HDM parameters, as the SM prediction of $\mu_{\gamma\gamma}$ aligns well with its measurement. This implies that we should have $\sin(\alpha - \beta) \approx 1$ (or equivalently, $\cos(\alpha - \beta) \approx 0$) to ensure that $T_{\gamma\gamma}^f$ and $T_{\gamma\gamma}^W$ are close to their SM values, and the contribution from the charged Higgs loops should be minimal. Additionally, we should have $\cos\theta'_2 \approx 1$ (or equivalently, $\sin\theta'_2 \approx 0$) to ensure that the ZW^+W^- coupling does not deviate too much from its SM value.

With the aforementioned approximations, we can first determine the contribution from charged Higgs loops. In the left panel of Figure 3, we present the 1σ and 2σ allowed regions for the parameters m_{H^\pm} and $\lambda_{hH^+H^-}$, with constraints derived from $\mu_{Z\gamma}$ (blue) and $\mu_{\gamma\gamma}$ (red). Clearly, reconciliation is only possible within the 2σ allowed regions, which correspond to a narrow parameter space. In the right panel of Figure 3, we compare the theoretical prediction (purple) with the experimental result (blue) for $\mu_{Z\gamma}$, where the theoretical contributions are obtained from the SM plus the charged Higgs contributions, with m_{H^\pm} and $\lambda_{hH^+H^-}$ constrained by $\mu_{\gamma\gamma}$. As observed, the theoretical prediction is nearly independent of the charged Higgs mass, and its value is very close to the SM prediction ($\mu_{Z\gamma}^{\text{SM}} = 1$), indicating that the charged Higgs contribution is negligible. Consequently, the scenario involving solely the charged Higgs can be ruled out.

Moving forward, we assess whether the contribution from the off-diagonal couplings of the Higgs and Z boson to W boson and charged Higgs can account for the observed excess in $\mu_{Z\gamma}$. This necessitates estimating the magnitude of $T_{Z\gamma}^{WH}$ as given in Eq. (17). To achieve this, we initially assign values to $\cos(\alpha - \beta)$ (or equivalently, $\sin(\alpha - \beta)$), g' , $\mathcal{Q}_2 - \mathcal{Q}_1$, $\cos\beta$

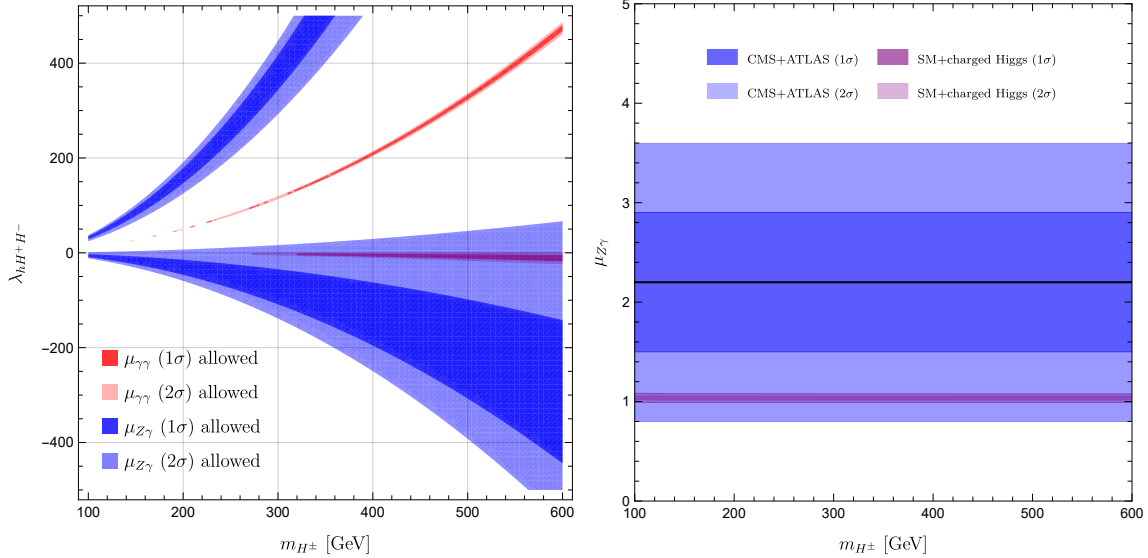


FIG. 3. Left: the 1σ and 2σ allowed regions for m_{H^\pm} and $\lambda_{hH^+H^-}$ with constraints from $\mu_{Z\gamma}$ (blue) and $\mu_{\gamma\gamma}$ (red). Right: the 1σ and 2σ allowed regions for $\mu_{Z\gamma}$, where the purple regions correspond to contributions from the SM plus merely charged Higgs with m_{H^\pm} and $\lambda_{hH^+H^-}$ allowed by $\mu_{\gamma\gamma}$, while the blue regions denote the experimental result jointly reported by CMS and ATLAS (the black horizontal line corresponds to the central value) [6].

(or equivalently, $\sin\beta$), and $\sin\theta'_2$. As discussed in the first paragraph of this subsection, to ensure that $T_{\gamma\gamma}^f$ and $T_{\gamma\gamma}^W$ do not deviate too much from their SM predictions, we should have $\cos(\alpha - \beta) \approx 0$ and $\sin\theta'_2 \approx 0$. What is more, the constraints from the B observables in our previous work suggest that $\tan\beta < 28$ and $g' > 10^{-2}$ [42]. The large upper limit of $\tan\beta$ suggests that $\cos\beta$ should be small, whereas g' is expected to remain sufficiently small to preserve the perturbative nature of the $U(1)$ gauge theory. Furthermore, considering the naturalness, it is reasonable to assume that $\mathcal{Q}_2 - \mathcal{Q}_1$ is of $\mathcal{O}(1)$. While satisfying these conditions and simultaneously hoping that $T_{Z\gamma}^{WH}$ is as large as possible, we assume that $\cos(\alpha - \beta) \sim \cos\beta \sim \sin\theta'_2 \sim \mathcal{O}(10^{-1})$ and $g' \sim (\mathcal{Q}_2 - \mathcal{Q}_1) \sim \mathcal{O}(1)$. With these assumptions, we can conservatively estimate:

$$a \equiv g'(\mathcal{Q}_2 - \mathcal{Q}_1) \cos(\alpha - \beta) \sin\beta \cos\beta \sin\theta'_2 \sim \mathcal{O}(10^{-3}). \quad (26)$$

To make a maximum estimate on $T_{Z\gamma}^{WH}$, let us assume that $|a|$ is close to the margin of $\mathcal{O}(10^{-2})$, say, $|a| = 0.01$. With this entry, we plot the magnitude of $T_{Z\gamma}^{WH}$ as a function of m_{H^\pm} in Figure 4. Obviously, $T_{Z\gamma}^{WH}$ decreases as m_{H^\pm} increases, and the magnitude of which can only reach $\mathcal{O}(10^{-8})$, comparable to that of the b quark loops in the SM (cf. the value of

$T_{Z\gamma}^{b,\text{SM}}$ in Eq. (22)), which is one and two orders of magnitude smaller than that of the t quark loops and W loops, respectively. Therefore, we can safely conclude that the contribution from the off-diagonal couplings of the Higgs and Z boson to W boson and charged Higgs is insufficient to explain the excess of the measured $\mu_{Z\gamma}$.

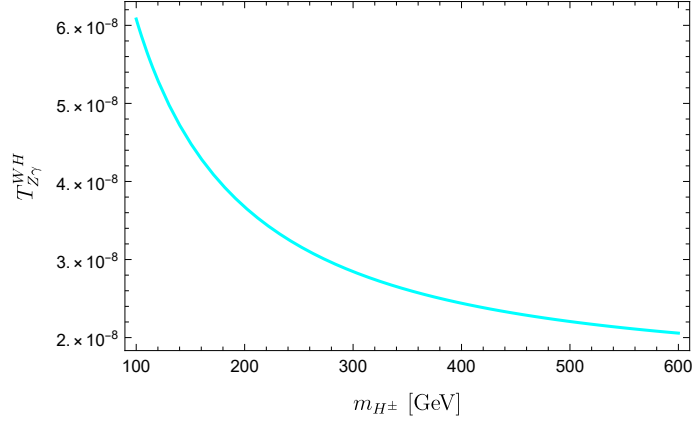


FIG. 4. The magnitude of $T_{Z\gamma}^{WH}$ as a function of $m_{H\pm}$ with input $|a| = 0.01$.

Lastly, let us check if the measured $\mu_{Z\gamma}$ excess can be mitigated by corrections to the Z boson-fermion vertices. Given that the top quark dominates contributions from the fermion loops, particular emphasis is placed on the correction from the $t\bar{t}Z$ vertex. Observing the numerical results of $T_{Z\gamma}^{W,\text{SM}}$ and $T_{Z\gamma}^{t,\text{SM}}$ in Eq. (22), since they are opposite in signs, combining these two terms implies a cancellation occurs, and the total amplitude must be smaller than that with the W loops alone. So if the $t\bar{t}Z$ vertex correction can flip the sign of $T_{Z\gamma}^{t,\text{SM}}$ and adjust its magnitude, the cancellation may transform into an enhancement. As a result, the original SM prediction is amplified within the FG2HDM framework. By adjusting the amount of the correction, we may be able to accommodate the measured $\mu_{Z\gamma}$ excess. The advantage of this approach is that it has no impact on the $\mu_{\gamma\gamma}$ at all. To implement this conjecture, let us first define:

$$C_V^f \equiv \frac{g_2}{2c_W}(I_f^3 - 2Q_f s_W^2) \cos \theta'_2 + \frac{g'}{2}(\mathcal{Q}_{fL} + \mathcal{Q}_{fR}) \sin \theta'_2. \quad (27)$$

With $\cos \theta'_2 \sim 1$ Eq. (27) can be further rewritten as $C_V^f = C_V^{f,\text{SM}} + \Delta C_V^f$, where $C_V^{f,\text{SM}} = \frac{g_2}{2c_W}(I_f^3 - 2Q_f s_W^2)$ and $\Delta C_V^f = \frac{g'}{2}(\mathcal{Q}_{fL} + \mathcal{Q}_{fR}) \sin \theta'_2$. Using $I_t^3 = 1/2$ and $Q_t = +2/3$ for the top quark, together with s_W and $\alpha(m_Z)$ from Table II, one gets $C_V^{t,\text{SM}} \simeq 0.071$. Moreover, by making use of the power counting for g' , $\mathcal{Q}_{tL} + \mathcal{Q}_{tR}$ (similar to $\mathcal{Q}_2 - \mathcal{Q}_1$), and $\sin \theta'_2$, one can roughly estimate that $\Delta C_V^t \sim \mathcal{O}(10^{-1})$, i.e., ΔC_V^t has the same order of magnitude as

$C_V^{t,SM}$. Our remaining work is to adjust the amount of the parameter ΔC_V^t to render the theoretical prediction consistent with the measurement of $\mu_{Z\gamma}$. In Figure 5 we depict the theoretical prediction of $\mu_{Z\gamma}$ as a function of ΔC_V^t (green solid line), which is compared to the 1σ and 2σ measured ones (blue regions) given by ATLAS and CMS [6]. It is shown that, when $\Delta C_V^t \in [-1.14, 0.13]$ the prediction can accommodate the measured $\mu_{Z\gamma}$ at the 2σ level and, when $\Delta C_V^t \in [-0.89, -0.28]$ the prediction can accommodate the same even at the 1σ level. This approach, if successful, could provide a viable explanation for the discrepancy observed in $\mu_{Z\gamma}$ while maintaining consistency with the $\mu_{\gamma\gamma}$. Further numerical analysis and experimental verification will be crucial to confirm the validity of this model adjustment.

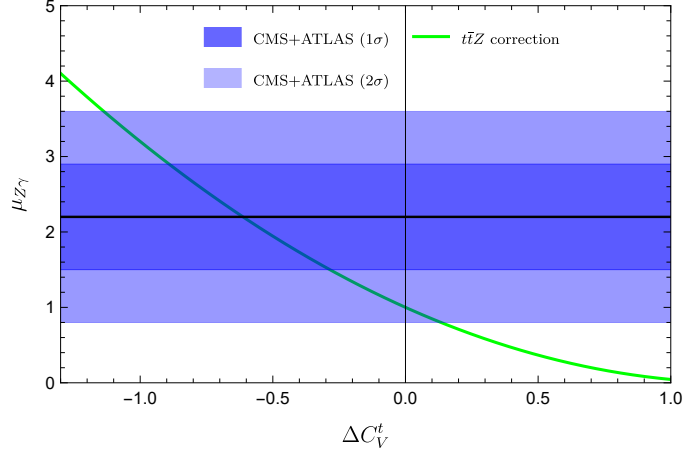


FIG. 5. The theoretical prediction of $\mu_{Z\gamma}$ as a function of ΔC_V^t (green solid line), in comparison with the measured one (blue regions) given by ATLAS and CMS [6].

To our knowledge, the most stringent constraints stem from two aspects: the top quark observables and the FCNC process $b \rightarrow s\ell^+\ell^-$. Regarding the former, both the CMS [46] and ATLAS [47, 48] collaborations have measured the differential and/or inclusive production cross sections of $t\bar{t}Z$ at the LHC, and the production of single top quarks and anti-top quarks via the t -channel exchange of a virtual W boson has been measured by ATLAS [49]. All of these measurements are in good agreement with their SM predictions. These measurements can be used to establish limits on the Wilson coefficients within the framework of the SM effective field theory (SMEFT) [50–52]. By leveraging the matching between ΔC_V^t and the SMEFT Wilson coefficients [53]:

$$\Delta C_V^t = \frac{g_2 v^2}{2\Lambda^2 c_W} \text{Re} \left[-C_{\varphi u}^{33} - C_{\varphi Q}^{(1,33)} + C_{\varphi Q}^{(3,33)} \right], \quad (28)$$

where $C_{\varphi u}$, $C_{\varphi Q}^{(1)}$, and $C_{\varphi Q}^{(3)}$ are the coefficients of the operators

$$\begin{aligned}\mathcal{O}_{\varphi u} &\equiv (\varphi^\dagger i \overleftrightarrow{D}_\mu \varphi) (\bar{u} \gamma^\mu u), \\ \mathcal{O}_{\varphi Q}^{(1)} &\equiv (\varphi^\dagger i \overleftrightarrow{D}_\mu \varphi) (\bar{Q} \gamma^\mu Q), \\ \mathcal{O}_{\varphi Q}^{(3)} &\equiv (\varphi^\dagger i \overleftrightarrow{D}_\mu \tau^I \varphi) (\bar{Q} \gamma^\mu \tau^I Q),\end{aligned}\tag{29}$$

respectively, one can determine the allowed range for ΔC_V^t . To estimate the maximum value of ΔC_V^t , we adopt $C_{\varphi t}^{33}/\Lambda^2 \in [-2.2, 1.6]$ from ATLAS (which corresponds to a 95% CL interval, with Λ being the NP scale set to 1 TeV, and the result is derived assuming one coefficient is non-zero at a time) [48]. Using Eq. (28) we find $\Delta C_V^t \in [-0.036, 0.049]$, which is approximately one order of magnitude smaller than the 1σ interval required to reconcile the measured $\mu_{Z\gamma}$. As for the latter, ΔC_V^t contributes to $b \rightarrow s\ell^+\ell^-$ by inserting the $t\bar{t}Z$ vertex into the Z -penguin diagram, by matching onto the low-energy effective coefficients $C_{9,10}$ relevant to $b \rightarrow s\ell^+\ell^-$ [54], one obtains $\Delta C_V^t \in [-0.05, 0.015] \cup [0.01, 0.05]$. Similar to the former case, these ranges are also too small to account for the 1σ interval of $\mu_{Z\gamma}$.

C. Discussion

From the numerical analysis presented above, we observe that while the FG2HDM offers two potentially viable mechanisms to enhance $\mu_{Z\gamma}$ without altering $\mu_{\gamma\gamma}$, the small values of the model parameters combined with the stringent constraints from other processes lead to an inability to account for the observed excess in $\mu_{Z\gamma}$ at the 1σ level. Consequently, it is not feasible to resolve this discrepancy utilizing only the particles currently included in the FG2HDM, which implies the necessity for a model extension.

An alternative approach is to introduce novel fermions to the model, whose couplings to the Z boson have not been constrained by existing measurements, thereby allowing us to align them with the measured $\mu_{Z\gamma}$. As is well known, the fourth-generation heavy fermions have been ruled out by the $h \rightarrow \gamma\gamma$ decay [55–58], leaving light fermions to be possible. Given that these are light and charged particles, it is imperative to ensure they remain undetected in Z decays. A particle that meets these criteria is the technifermion, a building block of a QCD-like theory known as technicolor theory [59, 60]. In this framework, technifermions and their antiparticles are charged under a confining gauge symmetry, leading to their confinement within composite bound states, analogous to how quarks are confined within hadrons.

These bound states could be massive and elusive enough that they avoid constraints from Z decays. In certain models, these composite particles are also considered as candidates for dark matter, see, for example, Refs. [61–73] and the references therein. Various model configurations are possible; however, we opt for a simple scenario that imposes an $SU(N)_T$ gauge symmetry with two Dirac fermions, U and D , with quantum numbers assigned under the $SU(N)_T \times SU(3)_C \times SU(2)_L \times U(1)_Y \times U(1)'$ symmetries:

$$T_L = \begin{pmatrix} U_L \\ D_L \end{pmatrix} \sim (N, \mathbf{1}, \mathbf{2}, 0, X_{T_L}), \quad U_R \sim (N, \mathbf{1}, \mathbf{1}, \frac{1}{2}, X_{U_R}), \quad D_R \sim (N, \mathbf{1}, \mathbf{1}, -\frac{1}{2}, X_{D_R}). \quad (30)$$

The technifermions U and D contribute to $h \rightarrow Z\gamma$ and $h \rightarrow \gamma\gamma$ in a manner analogous to the SM fermions, resulting in expressions equivalent to those in Eqs. (14) and (19), with N_C replaced by N . For simplicity, we assume that U and D possess a degenerate mass denoted as m_f . In the left panel of Figure 6 we show the theoretical prediction for $\mu_{\gamma\gamma}$ as a function of the technifermion mass m_f , for technicolor numbers $N = 2, 3, 4, 5$, compared to the 1σ measured interval (red region). The numerical results indicate a preference for $N \geq 4$, with an increasing mass range observed for larger N .

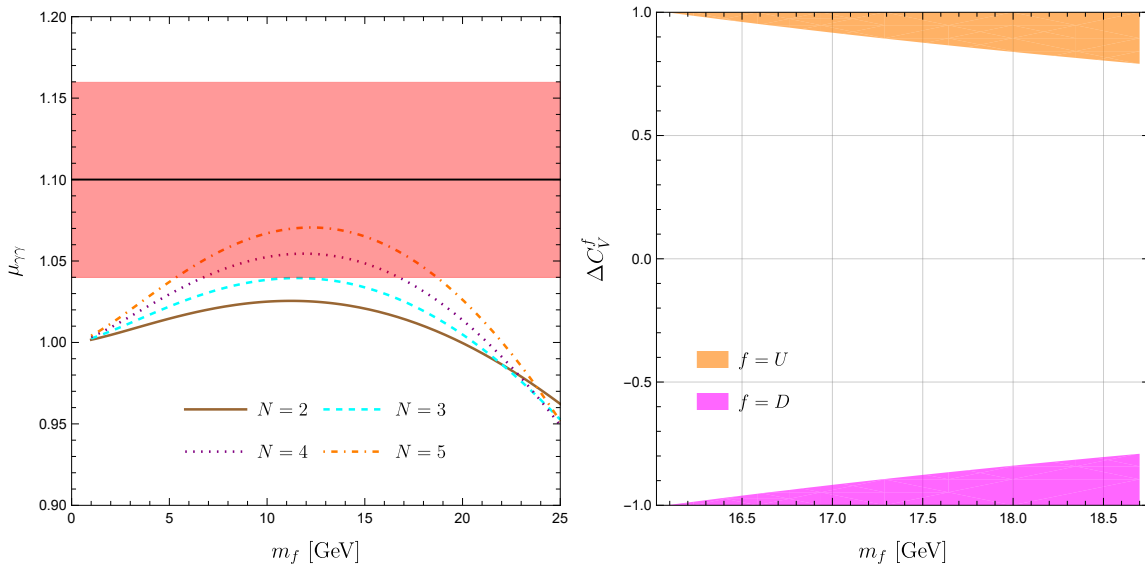


FIG. 6. Left: the theoretical prediction for $\mu_{\gamma\gamma}$ as a function of the technifermion mass m_f , for technicolor numbers $N = 2, 3, 4, 5$, compared to the 1σ measured interval (red region). Right: fixing $N = 5$, the $m_f - \Delta C_V^f$ regions required to reconcile the 1σ measured $\mu_{Z\gamma}$ interval for $f = U$ (orange region) and $f = D$ (magenta region).

In order to ascertain whether the aforementioned parameters of the technifermions al-

lowed by the measured $\mu_{\gamma\gamma}$ can also accommodate the measured $\mu_{Z\gamma}$ at the 1σ level, we substitute into Eq. (12) the contributions of the technifermions U and D , including the FG2HDM corrections to the Z boson-technifermion couplings. Our analysis reveals that the parameters meet the criteria only when $N \geq 5$. With N set to 5, we depict the 1σ measured $\mu_{Z\gamma}$ interval permitted regions for m_f and ΔC_V^f in the right panel of Figure 6. This analysis yields the range $m_f \in [16.0, 18.7]$ GeV, $\Delta C_V^U \in [0.8, 1.0]$ (orange region), and $\Delta C_V^D \in [-0.8, -1.0]$ (magenta region). Similar allowed regions for $m_f - \Delta C_V^f$ can be derived for $N > 5$, but they are not elaborated here.

V. CONCLUSION

In response to the 1.9σ deviation observed between the SM prediction and the measurement of the $h \rightarrow Z\gamma$ decay signal strength $\mu_{Z\gamma}$, as reported by ATLAS and CMS [6], this study endeavored to propose a potential resolution within the framework of the FG2HDM. Given the strong correlation between $h \rightarrow Z\gamma$ and $h \rightarrow \gamma\gamma$, which aligns well with the SM prediction, NP effects are required to enhance the former without altering the latter. This requirement can be met in the FG2HDM through two mechanisms: (i) introducing off-diagonal interactions, with Higgs and Z boson couple to charged Higgs and W boson, and (ii) introducing additional corrections to the Z boson-fermion vertices. With the prepared Lagrangian and Feynman rules for the FG2HDM in Appendix A, we calculated the amplitudes for both $h \rightarrow Z\gamma$ and $h \rightarrow \gamma\gamma$ decays. Our numerical analysis initially focused on establishing SM predictions for the branching ratios of these decays, followed by an in-depth examination of the FG2HDM corrections. We discovered that, due to the small parameters within the FG2HDM, the contribution from the off-diagonal couplings scenario was insufficient to account for the excess in the measured $\mu_{Z\gamma}$. Similarly, the constraints imposed by the top quark observables and the FCNC process $b \rightarrow s\ell^+\ell^-$ rendered the vertex correction scenario involving only SM fermions inadequate for the measured $\mu_{Z\gamma}$. To counteract this insufficiency, we incorporated two additional technifermions U and D into the FG2HDM, postulating them to be charged under an additional $SU(N)_T$ confining gauge symmetry, thus ensuring their confinements within the composite bound states, which could be massive and elusive that they avoid constraints from Z decays. We demonstrated as an example that with technicolor number $N = 5$, and a degenerate technifermion mass $m_f \in [16.0, 18.7]$ GeV, and

the Z boson-technifermion coupling corrections $\Delta C_V^U \in [0.8, 1.0]$ and $\Delta C_V^D \in [-0.8, -1.0]$, we can simultaneously reconcile the 1σ measured intervals of both $\mu_{Z\gamma}$ and $\mu_{\gamma\gamma}$.

ACKNOWLEDGEMENTS

This work is supported by NSFC under Grant Nos. 12475095 and U1932104, the Fundamental Research Funds for the Central Universities (11623330), and the 2024 Guangzhou Basic and Applied Basic Research Scheme Project for Maiden Voyage (2024A04J4190).

Appendix A: Lagrangian and Feynman rules

Since there involves at least one photon in both $h \rightarrow Z\gamma$ and $h \rightarrow \gamma\gamma$ decays, the propagators of the one-loop diagrams shall always be charged particles, see Figures 1 and 2. Therefore, to calculate the amplitudes we should first find out all of the Lagrangian that describe the interactions between the charged particles and the Higgs, Z boson, and photon. The formalisms of Feynman rules depend on the choice of gauge. In this paper we work in the unitary gauge, in which the Goldstones disappear and only physical particles participate the interactions. After scrutinizing the total Lagrangian provided in Ref. [42], we list the most relevant terms to calculate the amplitudes of $h \rightarrow Z\gamma$ and $h \rightarrow \gamma\gamma$ decays as follows,

$$\mathcal{L}_S = -\lambda_{hH^+H^-} v h H^+ H^-, \quad (\text{A1})$$

$$\mathcal{L}_{SF} = -\frac{1}{v} [\sin(\alpha - \beta) M_f - \cos(\alpha - \beta) N_f] h \bar{f} f, \quad (\text{A2})$$

$$\begin{aligned} \mathcal{L}_{SG} = & \frac{g_2^2 v}{2} \sin(\alpha - \beta) h W_\mu^+ W^{-\mu} - i e A_\mu (\partial^\mu H^+ H^- - \partial^\mu H^- H^+) + e^2 A_\mu A^\mu H^+ H^- \\ & - i \left[\left(\frac{g_2}{2} c_W - \frac{g_1}{2} s_W \right) \cos \theta'_2 + (\sin^2 \beta \mathcal{Q}_1 + \cos^2 \beta \mathcal{Q}_2) g' \sin \theta'_2 \right] Z_\mu (\partial^\mu H^+ H^- - \partial^\mu H^- H^+) \\ & - i \frac{g_2^2}{2} \cos(\alpha - \beta) \left[\partial^\mu h (W_\mu^+ H^- - W_\mu^- H^+) + h (\partial^\mu H^+ W_\mu^- - \partial^\mu H^- W_\mu^+) \right] \\ & + g_2 g' (\mathcal{Q}_2 - \mathcal{Q}_1) v \sin \beta \cos \beta \sin \theta'_2 Z^\mu (W_\mu^+ H^- + W_\mu^- H^+) \\ & + 2 g_2 s_W \left[\left(\frac{g_2}{2} c_W - \frac{g_1}{2} s_W \right) \cos \theta'_2 + (\sin^2 \beta \mathcal{Q}_1 + \cos^2 \beta \mathcal{Q}_2) g' \sin \theta'_2 \right] A_\mu Z^\mu H^+ H^- \\ & - \frac{g_2^2}{2} s_W \cos(\alpha - \beta) A^\mu (H^+ W_\mu^- + H^- W_\mu^+) h, \end{aligned} \quad (\text{A3})$$

$$\begin{aligned} \mathcal{L}_G = & i g_2 c_W \cos \theta'_2 \left[(\partial_\mu W_\nu^+ W^{-\mu} Z^\nu - \partial_\mu W_\nu^+ W^{-\nu} Z^\mu) - (\partial_\mu W_\nu^- W^{+\mu} Z^\nu - \partial_\mu W_\nu^- W^{+\nu} Z^\mu) \right. \\ & \left. + (\partial_\mu Z_\nu W^{+\mu} W^{-\nu} - \partial_\mu Z_\nu W^{-\mu} W^{+\nu}) \right] + i g_2 s_W \left[(\partial_\mu W_\nu^+ W^{-\mu} A^\nu - \partial_\mu W_\nu^+ W^{-\nu} A^\mu) \right. \end{aligned}$$

$$\begin{aligned}
& - (\partial_\mu W_\nu^- W^{+\mu} A^\nu - \partial_\mu W_\nu^- W^{+\nu} A^\mu) + (\partial_\mu A_\nu W^{+\mu} W^{-\nu} - \partial_\mu A_\nu W^{-\mu} W^{+\nu})] \\
& - g_2^2 s_W c_W \cos \theta_2' [2W_\mu^+ W^{-\mu} A^\nu Z_\nu - W_\mu^+ W^{-\nu} A_\nu Z^\mu - W_\nu^- W^{+\mu} A_\mu Z^\nu] \\
& - g_2^2 s_W^2 (W_\mu^+ W^{-\mu} A^\nu A_\nu - W_\mu^+ W^{-\nu} A_\nu A^\mu) , \tag{A4}
\end{aligned}$$

$$\begin{aligned}
\mathcal{L}_{FG} &= \frac{g_2 \cos \theta_2'}{c_W} Z_\mu \bar{f} [(I_f^3 - Q_f s_W^2) \gamma^\mu P_L - Q_f s_W^2 \gamma^\mu P_R] f \\
& + g' \sin \theta_2' Z_\mu \bar{f} [Q_{fL} \gamma^\mu P_L + Q_{fR} \gamma^\mu P_R] f + e Q_f A_\mu \bar{f} \gamma^\mu f . \tag{A5}
\end{aligned}$$

The first Lagrangian \mathcal{L}_S , which describes the interaction between the neutral and charged Higgs, is obtained by expressing the scalar potential (cf. Eq. (1)) in terms of physical fields, and their coupling reads

$$\begin{aligned}
\lambda_{hH^+H^-} &= \frac{1}{v} [\lambda_1 v_1 \sin \alpha \sin^2 \beta - \lambda_2 v_2 \cos \alpha \cos^2 \beta + v_1 \cos \beta (\lambda_3 \sin \alpha \cos \beta + \lambda_4 \cos \alpha \sin \beta) \\
& - v_2 \sin \beta (\lambda_3 \cos \alpha \sin \beta + \lambda_4 \sin \alpha \cos \beta)] . \tag{A6}
\end{aligned}$$

The second Lagrangian \mathcal{L}_{SF} is the Yukawa interactions, with M_f ($f = u, d, \ell$) being the diagonal mass matrices: $M_u = \text{diag}(m_u, m_c, m_t)$, $M_d = (m_d, m_s, m_b)$, and $M_\ell = (e, \mu, \tau)$. Here, M_f is diagonalized by a biunitary transformation:

$$M_f = \frac{1}{\sqrt{2}} U_{fL}^\dagger (v_1 Y_1^f + v_2 Y_2^f) U_{fR} , \tag{A7}$$

where Y_1^f and Y_2^f are Yukawa matrices, and U_{fL} and U_{fR} are unitary matrices. For convenience, we have also introduced the auxiliary matrices N_f , which are defined as

$$N_f = \frac{1}{\sqrt{2}} U_{fL}^\dagger (v_1 Y_2^f - v_2 Y_1^f) U_{fR} . \tag{A8}$$

To study the B anomalies in Ref. [42], we have assigned some specific $U(1)'$ quantum numbers for the fields so as to force the tree-level FCNC arising at the down-type quark sector. With such an assignments, the Yukawa matrices have the following textures:

$$\begin{aligned}
Y_1^u &= \begin{pmatrix} * & * & 0 \\ * & * & 0 \\ 0 & 0 & 0 \end{pmatrix} , & Y_2^u &= \begin{pmatrix} 0 & 0 & 0 \\ 0 & 0 & 0 \\ 0 & 0 & * \end{pmatrix} , & Y_1^d &= \begin{pmatrix} * & * & * \\ * & * & * \\ 0 & 0 & 0 \end{pmatrix} , & Y_2^d &= \begin{pmatrix} 0 & 0 & 0 \\ 0 & 0 & 0 \\ * & * & * \end{pmatrix} , \\
Y_1^\ell &= \begin{pmatrix} 0 & 0 & 0 \\ 0 & * & 0 \\ 0 & 0 & * \end{pmatrix} , & Y_2^\ell &= \begin{pmatrix} * & 0 & 0 \\ 0 & 0 & 0 \\ 0 & 0 & 0 \end{pmatrix} , \tag{A9}
\end{aligned}$$

where ‘*’ denotes an arbitrary non-zero number. Then the auxiliary matrices N_f have the following explicit forms:

$$\begin{aligned}
N_u &= -\frac{v_2}{v_1} \text{diag}(m_u, m_c, 0) + \frac{v_1}{v_2} \text{diag}(0, 0, m_t), \\
(N_d)_{ij} &= -\frac{v_2}{v_1} (M_d)_{ij} + \left(\frac{v_2}{v_1} + \frac{v_1}{v_2} \right) (V_{\text{CKM}}^\dagger)_{i3} (V_{\text{CKM}})_{3j} (M_d)_{jj}, \\
N_\ell &= -\frac{v_2}{v_1} \text{diag}(0, m_\mu, m_\tau) + \frac{v_1}{v_2} \text{diag}(m_e, 0, 0),
\end{aligned} \tag{A10}$$

where V_{CKM} denotes the Cabibbo-Kobayashi-Maskawa (CKM) matrix [74, 75]. The third Lagrangian \mathcal{L}_{SG} describes the interactions between the scalars and the gauge bosons, which is obtained by expanding the scalar kinetic terms with gauge bosons contained in the covariant derivatives. The quantities \mathcal{Q}_1 and \mathcal{Q}_2 denote respectively the $U(1)'$ charges of Φ_1 and Φ_2 , and s_W and c_W are separately short for $\sin\theta_W$ and $\cos\theta_W$. The fourth Lagrangian \mathcal{L}_G describes the interactions between the gauge bosons, which results from the vector field strength terms. The last Lagrangian \mathcal{L}_{FG} contains the interactions between the fermions and Z boson and photon, where I_f^3 stands for the third component of the weak isospin of a fermion doublet, Q_f denote the electric charge of a given fermion f , and \mathcal{Q}_{fL} and \mathcal{Q}_{fR} label the $U(1)'$ charge of a left-handed and right-handed fermion, respectively. It is also clear from Eq. (A5) that due to the $Z - Z'$ mixing there is an additional term that has the same Lorentz structure as the SM one, which therefore provides a correction to the original couplings. For more details of FG2HDM Lagrangian in different sectors, readers are referred to Ref. [42].

With the Lagrangian listed in Eqs. (A1)-(A5) at hand, obtaining the Feynman rules for the vertices is straightforward. Besides, the Feynman rules for the propagators of the charged Higgs, W boson, and fermions can be derived directly from the free Lagrangian that we do not show. Working in the unitary gauge, we summarize all the relevant vertices as well as propagators of FG2HDM that are necessary to calculate the amplitudes of $h \rightarrow Z\gamma$ and $h \rightarrow \gamma\gamma$ decays in Figure 7.

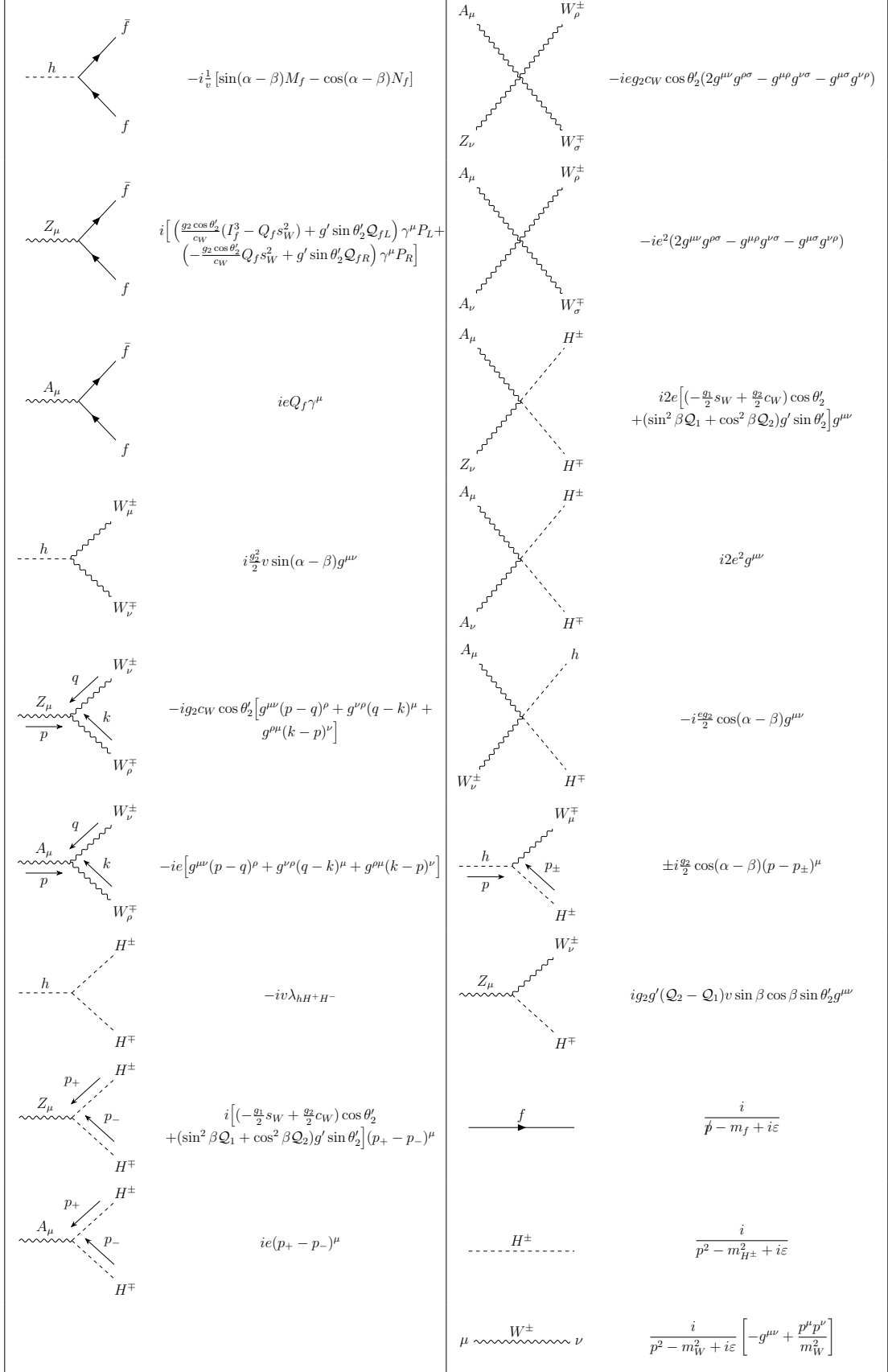


FIG. 7. Feynman rules for the relevant vertices and propagators in the unitary gauge.

Appendix B: Scalar functions

In this appendix, we show the analytical expressions for the scalar functions appearing in Sec. III A and III B.

$$\Lambda(m_a^2; m_b, m_c) = \frac{1}{m_a^2} \lambda^{\frac{1}{2}}(m_a^2, m_b^2, m_c^2) \text{Log} \left(\frac{\lambda^{\frac{1}{2}}(m_a^2, m_b^2, m_c^2) - m_a^2 + m_b^2 + m_c^2}{2m_b m_c} \right), \quad (\text{B1})$$

$$C_0(m_Z^2, 0, m_h^2, m_i^2, m_i^2, m_i^2) = \frac{1}{2(m_h^2 - m_Z^2)} \left[\text{Log}^2 \left(\frac{\sqrt{-m_h^2(4m_i^2 - m_h^2)} + 2m_i^2 - m_h^2}{2m_i^2} \right) - \text{Log}^2 \left(\frac{\sqrt{-m_Z^2(4m_i^2 - m_Z^2)} + 2m_i^2 - m_Z^2}{2m_i^2} \right) \right], \quad (\text{B2})$$

$$C_0(0, 0, m_h^2, m_i^2, m_i^2, m_i^2) = \frac{1}{2m_h^2} \text{Log}^2 \left(\frac{\sqrt{-m_h^2(4m_i^2 - m_h^2)} + 2m_i^2 - m_h^2}{2m_i^2} \right), \quad (\text{B3})$$

$$C_0(0, m_h^2, m_Z^2, m_i^2, m_i^2, m_j^2) = \frac{1}{m_h^2 - m_Z^2} \left\{ -\text{DiLog} \left[\frac{2(m_h^2 + \Delta_{ij})}{m_h^2 + \Delta_{ij} - \lambda^{\frac{1}{2}}(m_h^2, m_i^2, m_j^2)}, m_h^2 + \Delta_{ij} \right] - \text{DiLog} \left[\frac{2(m_h^2 + \Delta_{ij})}{m_h^2 + \Delta_{ij} + \lambda^{\frac{1}{2}}(m_h^2, m_i^2, m_j^2)}, -(m_h^2 + \Delta_{ij}) \right] + \text{DiLog} \left[\frac{2\Delta_{ij}}{m_h^2 + \Delta_{ij} - \lambda^{\frac{1}{2}}(m_h^2, m_i^2, m_j^2)}, \Delta_{ij} \right] + \text{DiLog} \left[\frac{2\Delta_{ij}}{m_h^2 + \Delta_{ij} + \lambda^{\frac{1}{2}}(m_h^2, m_i^2, m_j^2)}, -\Delta_{ij} \right] - (m_h \rightarrow m_Z) \right\}, \quad (\text{B4})$$

where $\Delta_{ij} = m_i^2 - m_j^2$, $\lambda(a, b, c) = a^2 + b^2 + c^2 - 2ab - 2ac - 2bc$ is the usual Källén function, and $\text{DiLog}[a, b]$ is a function defined in *Package-X* [44].

Appendix C: Kinematics

Both $h(p) \rightarrow Z(p_1)\gamma(p_2)$ and $h(p) \rightarrow \gamma(p_1)\gamma(p_2)$ are processes of two-body decays, the differential decay width of which reads

$$d\Gamma = \frac{1}{2m_h} |\mathcal{M}_X|^2 d\Phi_2, \quad (\text{C1})$$

where \mathcal{M}_X denotes the amplitude, and $d\Phi_2$ is the two-body decay phase space given by

$$d\Phi_2 = \frac{|\vec{p}_1|}{16\pi^2 m_h} d\Omega. \quad (\text{C2})$$

Here, $|\vec{p}_1| = \lambda^{1/2}(m_h^2, m_1^2, m_2^2)/2m_h$, which is equal to $(m_h^2 - m_Z^2)/2m_h$ for $h \rightarrow Z\gamma$ and $m_h/2$ for $h \rightarrow \gamma\gamma$, respectively; $d\Omega = d\phi_1 d\cos\theta_1$ being the solid angle of particle 1 in the final state, which, after integration, yields 4π . To calculate the decay width or branching ratio of the two processes, one has to sum over the spins of Z boson and photon in the final state:

$$\begin{aligned} \sum_{\lambda_1, \lambda_2} |\mathcal{M}_X|^2 &= |T_X|^2 (p_2^\mu p_1^\nu - p_1 \cdot p_2 g^{\mu\nu}) (p_2^\alpha p_1^\beta - p_1 \cdot p_2 g^{\alpha\beta}) \\ &\times \sum_{\lambda_1, \lambda_2} [\epsilon_\mu^*(p_1, \lambda_1) \epsilon_\alpha(p_1, \lambda_1)] [\epsilon_\nu^*(p_2, \lambda_2) \epsilon_\beta(p_2, \lambda_2)]. \end{aligned} \quad (\text{C3})$$

For $X = Z\gamma$, one has

$$\sum_{\lambda_1, \lambda_2} [\epsilon_\mu^*(p_1, \lambda_1) \epsilon_\alpha(p_1, \lambda_1)] [\epsilon_\nu^*(p_2, \lambda_2) \epsilon_\beta(p_2, \lambda_2)] = \left(-g_{\mu\alpha} + \frac{p_{1\mu} p_{1\alpha}}{m_Z^2} \right) (-g_{\nu\beta}). \quad (\text{C4})$$

Substituting this back to Eq. (C3) and divided by the total decay width of Higgs Γ_h , yields the branching fraction for $h \rightarrow Z\gamma$,

$$\mathcal{B}(h \rightarrow Z\gamma) = \frac{m_h^3}{32\pi\Gamma_h} \left(1 - \frac{m_Z^2}{m_h^2} \right)^3 |T_{Z\gamma}|^2. \quad (\text{C5})$$

Similarly, for $X = \gamma\gamma$, one has

$$\sum_{\lambda_1, \lambda_2} [\epsilon_\mu^*(p_1, \lambda_1) \epsilon_\alpha(p_1, \lambda_1)] [\epsilon_\nu^*(p_2, \lambda_2) \epsilon_\beta(p_2, \lambda_2)] = (-g_{\mu\alpha}) (-g_{\nu\beta}), \quad (\text{C6})$$

and the branching fraction for $h \rightarrow \gamma\gamma$ reads

$$\mathcal{B}(h \rightarrow \gamma\gamma) = \frac{m_h^3}{64\pi\Gamma_h} |T_{\gamma\gamma}|^2. \quad (\text{C7})$$

In deriving Eq. (C7), since there are two identical photons in the final state, an extra $1/2$ factor has been taken into account.

-
- [1] G. Aad *et al.* (ATLAS), *Phys. Lett. B* **716**, 1 (2012), arXiv:1207.7214 [hep-ex].
 - [2] S. Chatrchyan *et al.* (CMS), *Phys. Lett. B* **716**, 30 (2012), arXiv:1207.7235 [hep-ex].
 - [3] S. Chatrchyan *et al.* (CMS), *JHEP* **06**, 081 (2013), arXiv:1303.4571 [hep-ex].
 - [4] G. Aad *et al.* (ATLAS), *Phys. Lett. B* **809**, 135754 (2020), arXiv:2005.05382 [hep-ex].
 - [5] A. Tumasyan *et al.* (CMS), *JHEP* **05**, 233 (2023), arXiv:2204.12945 [hep-ex].
 - [6] G. Aad *et al.* (ATLAS, CMS), *Phys. Rev. Lett.* **132**, 021803 (2024), arXiv:2309.03501 [hep-ex].

- [7] M. Spira, A. Djouadi, and P. M. Zerwas, *Phys. Lett. B* **276**, 350 (1992).
- [8] T. Gehrmann, S. Guns, and D. Kara, *JHEP* **09**, 038 (2015), [arXiv:1505.00561 \[hep-ph\]](#).
- [9] R. Bonciani, V. Del Duca, H. Frellesvig, J. M. Henn, F. Moriello, and V. A. Smirnov, *JHEP* **08**, 108 (2015), [arXiv:1505.00567 \[hep-ph\]](#).
- [10] F. Buccioni, F. Devoto, A. Djouadi, J. Ellis, J. Quevillon, and L. Tancredi, *Phys. Lett. B* **851**, 138596 (2024), [arXiv:2312.12384 \[hep-ph\]](#).
- [11] Z.-Q. Chen, L.-B. Chen, C.-F. Qiao, and R. Zhu, *Phys. Rev. D* **110**, L051301 (2024), [arXiv:2404.11441 \[hep-ph\]](#).
- [12] W.-L. Sang, F. Feng, and Y. Jia, (2024), [arXiv:2405.03464 \[hep-ph\]](#).
- [13] S. Panghal and B. Mukhopadhyaya, (2023), [arXiv:2310.04136 \[hep-ph\]](#).
- [14] G. Lichtenstein, M. A. Schmidt, G. Valencia, and R. R. Volkas, (2023), [arXiv:2312.09409 \[hep-ph\]](#).
- [15] T. T. Hong, V. K. Le, L. T. T. Phuong, N. . C. Hoi, N. T. K. Ngan, and N. H. T. Nha, *PTEP* **2024**, 033B04 (2024), [Erratum: *PTEP* 2024, 059201 (2024)], [arXiv:2312.11045 \[hep-ph\]](#).
- [16] R. Boto, D. Das, J. C. Romao, I. Saha, and J. P. Silva, *Phys. Rev. D* **109**, 095002 (2024), [arXiv:2312.13050 \[hep-ph\]](#).
- [17] N. Das, T. Jha, and D. Nanda, *Phys. Rev. D* **109**, 115020 (2024), [arXiv:2402.01317 \[hep-ph\]](#).
- [18] K. Cheung and C. J. Ouseph, (2024), [arXiv:2402.05678 \[hep-ph\]](#).
- [19] X.-G. He, Z.-L. Huang, M.-W. Li, and C.-W. Liu, (2024), [arXiv:2402.08190 \[hep-ph\]](#).
- [20] B. A. Ouazghour, M. Chabab, and K. Goure, (2024), [arXiv:2403.07722 \[hep-ph\]](#).
- [21] A. Arhrib, K. H. Phan, V. Q. Tran, and T.-C. Yuan, (2024), [arXiv:2405.03127 \[hep-ph\]](#).
- [22] A. I. Hernández-Juárez, R. Gaitán, and R. Martinez, (2024), [arXiv:2405.03094 \[hep-ph\]](#).
- [23] C. Grojean, G. Guedes, J. Roosmale Nepveu, and G. M. Salla, (2024), [arXiv:2405.20371 \[hep-ph\]](#).
- [24] H.-c. Hu, Z.-Y. Zhang, N.-Y. Zhu, and H.-X. Chen, *Chin. Phys. C* **48**, 093101 (2024), [arXiv:2406.00946 \[hep-ph\]](#).
- [25] A. Arhrib, R. Benbrik, L. Rahili, S. Semlali, and B. Taki, *Eur. Phys. J. C* **84**, 799 (2024), [arXiv:2406.13001 \[hep-ph\]](#).
- [26] K. H. Phan, D. T. Tran, and T. H. Nguyen, (2024), [arXiv:2406.15749 \[hep-ph\]](#).
- [27] S. Israr and M. Rehman, (2024), [arXiv:2407.01210 \[hep-ph\]](#).
- [28] K. Mantzaropoulos, (2024), [arXiv:2407.09145 \[hep-ph\]](#).

- [29] R. Boto, P. N. Figueiredo, J. C. Romão, and J. a. P. Silva, (2024), [arXiv:2407.15933 \[hep-ph\]](#).
- [30] J. F. Gunion, H. E. Haber, G. L. Kane, and S. Dawson, *The Higgs Hunter's Guide*, Vol. 80 (2000).
- [31] A. Djouadi, *Phys. Rept.* **457**, 1 (2008), [arXiv:hep-ph/0503172](#).
- [32] S. Navas *et al.* (Particle Data Group), *Phys. Rev. D* **110**, 030001 (2024).
- [33] G. C. Branco, P. M. Ferreira, L. Lavoura, M. N. Rebelo, M. Sher, and J. P. Silva, *Phys. Rept.* **516**, 1 (2012), [arXiv:1106.0034 \[hep-ph\]](#).
- [34] D. Fontes, J. C. Romão, and J. a. P. Silva, *JHEP* **12**, 043 (2014), [arXiv:1408.2534 \[hep-ph\]](#).
- [35] G. Aad *et al.* (ATLAS), *Phys. Lett. B* **732**, 8 (2014), [arXiv:1402.3051 \[hep-ex\]](#).
- [36] S. Chatrchyan *et al.* (CMS), *Phys. Lett. B* **726**, 587 (2013), [arXiv:1307.5515 \[hep-ex\]](#).
- [37] G. C. Branco, W. Grimus, and L. Lavoura, *Phys. Lett. B* **380**, 119 (1996), [arXiv:hep-ph/9601383](#).
- [38] A. Celis, J. Fuentes-Martin, M. Jung, and H. Serodio, *Phys. Rev. D* **92**, 015007 (2015), [arXiv:1505.03079 \[hep-ph\]](#).
- [39] A. Ordell, R. Pasechnik, H. Serôdio, and F. Nottensteiner, *Phys. Rev. D* **100**, 115038 (2019), [arXiv:1909.05548 \[hep-ph\]](#).
- [40] A. Ordell, R. Pasechnik, and H. Serôdio, *Phys. Rev. D* **102**, 035016 (2020), [arXiv:2006.08676 \[hep-ph\]](#).
- [41] P. M. Ferreira, F. F. Freitas, J. a. Gonçalves, A. P. Morais, R. Pasechnik, and V. Vatellis, *Phys. Rev. D* **106**, 075017 (2022), [arXiv:2202.13153 \[hep-ph\]](#).
- [42] Q. Wen and F. Xu, (2024), [arXiv:2408.03848 \[hep-ph\]](#).
- [43] L. Bergstrom and G. Hulth, *Nucl. Phys. B* **259**, 137 (1985), [Erratum: *Nucl.Phys.B* 276, 744–744 (1986)].
- [44] H. H. Patel, *Comput. Phys. Commun.* **197**, 276 (2015), [arXiv:1503.01469 \[hep-ph\]](#).
- [45] D. de Florian *et al.* (LHC Higgs Cross Section Working Group), **2/2017** (2016), [10.23731/CYRM-2017-002](#), [arXiv:1610.07922 \[hep-ph\]](#).
- [46] A. M. Sirunyan *et al.* (CMS), *JHEP* **03**, 056 (2020), [arXiv:1907.11270 \[hep-ex\]](#).
- [47] G. Aad *et al.* (ATLAS), *Eur. Phys. J. C* **81**, 737 (2021), [arXiv:2103.12603 \[hep-ex\]](#).
- [48] G. Aad *et al.* (ATLAS), *JHEP* **07**, 163 (2024), [arXiv:2312.04450 \[hep-ex\]](#).
- [49] G. Aad *et al.* (ATLAS), *JHEP* **05**, 305 (2024), [arXiv:2403.02126 \[hep-ex\]](#).
- [50] W. Buchmuller and D. Wyler, *Nucl. Phys. B* **268**, 621 (1986).

- [51] B. Grzadkowski, M. Iskrzynski, M. Misiak, and J. Rosiek, *JHEP* **10**, 085 (2010), [arXiv:1008.4884 \[hep-ph\]](#).
- [52] I. Brivio and M. Trott, *Phys. Rept.* **793**, 1 (2019), [arXiv:1706.08945 \[hep-ph\]](#).
- [53] J. A. Aguilar-Saavedra, *Nucl. Phys. B* **812**, 181 (2009), [arXiv:0811.3842 \[hep-ph\]](#).
- [54] Q. Wen and F. Xu, *Phys. Rev. D* **108**, 095038 (2023), [arXiv:2305.19038 \[hep-ph\]](#).
- [55] N. Chen and H.-J. He, *JHEP* **04**, 062 (2012), [arXiv:1202.3072 \[hep-ph\]](#).
- [56] O. Eberhardt, G. Herbert, H. Lacker, A. Lenz, A. Menzel, U. Nierste, and M. Wiebusch, *Phys. Rev. Lett.* **109**, 241802 (2012), [arXiv:1209.1101 \[hep-ph\]](#).
- [57] A. Djouadi and A. Lenz, *Phys. Lett. B* **715**, 310 (2012), [arXiv:1204.1252 \[hep-ph\]](#).
- [58] E. Kuflik, Y. Nir, and T. Volansky, *Phys. Rev. Lett.* **110**, 091801 (2013), [arXiv:1204.1975 \[hep-ph\]](#).
- [59] S. Weinberg, *Phys. Rev. D* **13**, 974 (1976), [Addendum: *Phys.Rev.D* 19, 1277–1280 (1979)].
- [60] L. Susskind, *Phys. Rev. D* **20**, 2619 (1979).
- [61] T. A. Ryttov and F. Sannino, *Phys. Rev. D* **78**, 115010 (2008), [arXiv:0809.0713 \[hep-ph\]](#).
- [62] T. Hambye and M. H. G. Tytgat, *Phys. Lett. B* **683**, 39 (2010), [arXiv:0907.1007 \[hep-ph\]](#).
- [63] Y. Bai and R. J. Hill, *Phys. Rev. D* **82**, 111701 (2010), [arXiv:1005.0008 \[hep-ph\]](#).
- [64] A. Belyaev, M. T. Frandsen, S. Sarkar, and F. Sannino, *Phys. Rev. D* **83**, 015007 (2011), [arXiv:1007.4839 \[hep-ph\]](#).
- [65] R. Lewis, C. Pica, and F. Sannino, *Phys. Rev. D* **85**, 014504 (2012), [arXiv:1109.3513 \[hep-ph\]](#).
- [66] M. Frigerio, A. Pomarol, F. Riva, and A. Urbano, *JHEP* **07**, 015 (2012), [arXiv:1204.2808 \[hep-ph\]](#).
- [67] M. R. Buckley and E. T. Neil, *Phys. Rev. D* **87**, 043510 (2013), [arXiv:1209.6054 \[hep-ph\]](#).
- [68] S. Bhattacharya, B. Melić, and J. Wudka, *JHEP* **02**, 115 (2014), [arXiv:1307.2647 \[hep-ph\]](#).
- [69] A. Hietanen, R. Lewis, C. Pica, and F. Sannino, *JHEP* **07**, 116 (2014), [arXiv:1404.2794 \[hep-lat\]](#).
- [70] Y. Hochberg, E. Kuflik, H. Murayama, T. Volansky, and J. G. Wacker, *Phys. Rev. Lett.* **115**, 021301 (2015), [arXiv:1411.3727 \[hep-ph\]](#).
- [71] A. Carmona and M. Chala, *JHEP* **06**, 105 (2015), [arXiv:1504.00332 \[hep-ph\]](#).
- [72] Y. Hochberg, E. Kuflik, and H. Murayama, *JHEP* **05**, 090 (2016), [arXiv:1512.07917 \[hep-ph\]](#).
- [73] G. D. Kribs and E. T. Neil, *Int. J. Mod. Phys. A* **31**, 1643004 (2016), [arXiv:1604.04627 \[hep-ph\]](#).

[74] N. Cabibbo, *Phys. Rev. Lett.* **10**, 531 (1963).

[75] M. Kobayashi and T. Maskawa, *Prog. Theor. Phys.* **49**, 652 (1973).